Computer simulation of bottle-brush polymers with flexible backbone: Good solvent versus theta solvent conditions

Panagiotis E. Theodorakis, Hsiao-Ping Hsu, Wolfgang Paul, and Kurt Binder

Computer simulation of bottle-brush polymers with flexible backbone: Good solvent versus theta solvent conditions

Panagiotis E. Theodorakis,[1,2,3,4,a)] Hsiao-Ping Hsu,[1,b)] Wolfgang Paul,[5,c)] and Kurt Binder[1,d)]

[1]*Institut für Physik, Johannes Gutenberg-Universität Mainz, Staudinger Weg 7, D-55099 Mainz, Germany*
[2]*Faculty of Physics, University of Vienna, Boltzmanngasse 5, A-1090 Vienna, Austria*
[3]*Institute for Theoretical Physics and Center for Computational Materials Science (CMS), Technical University of Vienna, Hauptstraße 8-10, A-1040 Vienna, Austria*
[4]*Vienna Computational Materials' Laboratory, Sensengasse 8/12, A-1090 Vienna, Austria*
[5]*Theoretische Physik, Martin Luther Universität Halle-Wittenberg, von Seckendorffplatz 1, 06120 Halle, Germany*

By molecular dynamics simulation of a coarse-grained bead-spring-type model for a cylindrical molecular brush with a backbone chain of N_b effective monomers to which with grafting density σ side chains with N effective monomers are tethered, several characteristic length scales are studied for variable solvent quality. Side chain lengths are in the range $5 \leq N \leq 40$, backbone chain lengths are in the range $50 \leq N_b \leq 200$, and we perform a comparison to results for the bond fluctuation model on the simple cubic lattice (for which much longer chains are accessible, $N_b \leq 1027$, and which corresponds to an athermal, very good, solvent). We obtain linear dimensions of the side chains and the backbone chain and discuss their N-dependence in terms of power laws and the associated effective exponents. We show that even at the theta point the side chains are considerably stretched, their linear dimension depending on the solvent quality only weakly. Effective persistence lengths are extracted both from the orientational correlations and from the backbone end-to-end distance; it is shown that different measures of the persistence length (which would all agree for Gaussian chains) are not mutually consistent with each other and depend distinctly both on N_b and the solvent quality. A brief discussion of pertinent experiments is given. © *2011 American Institute of Physics.*
[doi:10.1063/1.3656072]

I. INTRODUCTION

Macromolecules which consist of a "backbone" polymer, to which flexible or stiff side chains are grafted, the so-called "bottle-brush polymers," find very great interest recently (see Refs. 1–6 for reviews). Varying the chemical nature of both the backbone chain and the side chains, their chain lengths (N_b, N) and the grafting density σ, the structure of these cylindrical molecular brushes can be widely varied. That is, their local "thickness" as measured by the cross-sectional radius R_c or linear dimensions of individual side chains can be varied as well as their local "stiffness," traditionally measured by "the" persistence length l_p,[6–9] and their effective contour length L_c. Here, we use quotation marks with respect to "the" persistence length, because there is evidence, at least for the case of very good solvent conditions, that a unique persistence length measuring the "intrinsic" stiffness of a polymer cannot be defined in the standard fashion.[10,11] Now an intriguing observation[12] is the sensitivity of the large-scale structure of these bottle-brush polymers to solvent quality: one finds a thermally induced collapse of single macromolecules

from cylindrical brushes to spheres, in a very small temperature range, and it is speculated that these bottle-brushes could be useful as building blocks of "soft nanomachines."[12] We also note that biopolymers with comblike architecture are ubiquitous in nature (such as proteoglycans[13] or the aggrecan molecules that play a role in the soft lubricating layers in human joints.[14]), and probably in this context temperature and/or solvent quality (or pH value) are relevant parameters as well.

In view of these facts, a comprehensive clarification of how the properties of bottle-brush polymers depend on solvent quality clearly would be interesting. Although there are occasional experimental reports, how particular linear dimensions of these polymers scale in various solvents (e.g., Refs. 15–18), we are not aware of a systematic study of this problem. While work based on self-consistent field theory (SCFT) predicted already very early in Ref. 19 that the side chain gyration radius R_{gs} scales as $R_{gs} \propto N^{3/4}$ for good solvents and $R_{gs} \propto N^{2/3}$ for theta solvents, there is now evidence from experiment, simulation, and theory that these power laws apply if at all only for side chain lengths N of the order of 10^3, which are of no practical relevance: Experiments have only studied the range $N < 10^2$, and the range accessible in simulations[3,6,10,20–26] is similarly restricted. Numerical modeling applying the Scheutjens-Fleer version of SCFT has given clear evidence[27] that even within this mean-field

[a)]Electronic mail: panagiotis.theodorakis@univie.ac.at.
[b)]Electronic mail: hsu@uni-mainz.de.
[c)]Electronic mail: wolfgang.paul@physik.uni-halle.de.
[d)]Electronic mail: kurt.binder@uni-mainz.de.

approach $N \approx 10^3$ is needed to reach the regime, where the predicted power laws[19,28] apply. While the investigation of the scaling (self-similar) properties of bottle-brushes with extremely long backbone chains and very long side chains may be a challenging theoretical problem, it is of little relevance for the experimentally accessible systems, and clearly not in the focus of the present paper. Both the SCFT theories[19,27] and the scaling theories[29] consider ideal chains aiming to describe the behavior at the theta temperature, while previous simulations have almost exclusively considered the good solvent case only. Notable exceptions are studies of globule formation of bottle-brushes with very short side chains ($N = 4-12$) under poor solvent conditions[30] and the study of microphase separation of bottle-brushes with straight backbones in poor solvent.[31,32]

The present work intends to make a contribution to close this gap, by presenting a simulation study of a coarse-grained bead-spring (BS)-type model of bottle-brush polymers where the solvent quality is varied from very good solvent conditions to the theta point regime. In Sec. II, we shall describe the model and simulation technique, while in Sec. III we present our numerical results. In Sec. IV, a summary is given as well as an outlook on pertinent experiments.

II. MODEL AND SIMULATION METHOD

Extending our previous work on the simulation of bottle-brush polymers with rigid backbones,[31,32] we describe both the backbone chain and the side chains by a bead-spring model,[33–36] where all beads interact with a truncated and shifted Lennard-Jones (LJ) potential $U_{LJ}(r)$ and nearest neighbors bonded together along a chain also experience the finitely extensible nonlinear elastic potential $U_{FENE}(r)$, r being the distance between the beads. Thus

$$U_{LJ}(r) = 4\varepsilon_{LJ}\left[\left(\frac{\sigma_{LJ}}{r}\right)^{12} - \left(\frac{\sigma_{LJ}}{r}\right)^{6}\right] + C, \quad r \le r_c, \quad (1)$$

while $U_{LJ}(r > r_c) = 0$, and where $r_c = 2.5\sigma_{LJ}$. The constant C is defined such that $U_{LJ}(r = r_c)$ is continuous at the cutoff. Henceforth, units are chosen such that $\varepsilon_{LJ} = 1$, $\sigma_{LJ} = 1$, the Boltzmann constant $k_B = 1$, and in addition also the mass m_{LJ} of beads is chosen to be unity. The potential Eq. (1) acts between any pair of beads, irrespective of whether they are bonded or not. For bonded beads additionally the potential $U_{FENE}(r)$ acts,

$$U_{FENE}(r) = -\frac{1}{2}kr_0^2 \ln\left[1 - \left(\frac{r}{r_0}\right)^2\right], \quad 0 < r \le r_0, \quad (2)$$

while $U_{FENE}(r > r_0) = \infty$, and hence r_0 is the maximal distance that bonded beads can take. We use the standard choice[36] $r_0 = 1.5$ and $k = 30$. Related models have been used with great success to study the glassification of polymer melts formed from short chains[37] and to study the effects of solvent quality of polymer brushes on flat planar substrates.[38] For such models of brushes on a planar substrate, the implicit solvent model (Eq. (1)) has been compared with models using explicit solvent molecules, and it was found that the results are very similar.

Note that in our model there is no difference in interactions, irrespective of whether the considered beads are effective monomers of the backbone or of the side chains, implying that the polymer forming the backbone is either chemically identical to the polymers that are tethered as side chains to the backbone, or at least on coarse-grained length scales as considered here the backbone and side chain polymers are no longer distinct. There is also no difference between the bond linking the first monomer of a side chain to a monomer of the backbone and bonds between any other pairs of bonded monomers. Of course, our study does not address any effects due to a particular chemistry relating to the synthesis of these bottle-brush polymers, but as usually done[36,39,40] we address universal features of the conformational properties of these macromolecules.

There is one important distinction relating to our previous work[31,32] on bottle-brush polymers with rigid backbones: following Grest and Murat,[35] there the backbone was taken as an infinitely thin straight line in continuous space, thus allowing arbitrary values of the distances between neighboring grafting sites, and hence the grafting density σ could be continuously varied. For the present model, where we disregard any possible quenched disorder resulting from the grafting process, of course, the grafting density σ is quantized: we denote here by $\sigma = 1$ the case that every backbone monomer carries a side chain, $\sigma = 0.5$ means that every second backbone monomer has a side chain, etc. Chain lengths of side chains were chosen as $N = 5, 10, 20,$ and 40, while backbone chain lengths were chosen as $N_b = 50, 100,$ and 200, respectively.

It is obvious, of course, that for such short side chain lengths any interpretation of characteristic lengths in terms of power laws, such as $R_c \propto N^{\nu_{eff}}$, is a delicate matter, ν_{eff} being an "effective exponent" and characterizes only the specified range of rather small values of N and not the limit $N \to \infty$ considered by most theories.[2,19,27–29] Thus, the actual value of ν_{eff} is of limited interest, it only gives an indication to which part of an extended crossover region the data belong. However, we emphasize that (i) our range of N nicely corresponds to the range available in experiments.[1,4,15–18,26,41–43] (ii) The analysis in terms of power laws with effective exponents is a standard practice of experimentalists in this context (e.g., Refs. 1 and 17).

We recall that for linear chains, the theta temperature for the present (implicit solvent) model has been roughly estimated[44] as $T_\theta \approx 3.0$ (note, however, that there is still some uncertainty about the precise value of T_θ: for a similar model[45] the correct value of T_θ, $T_\theta \approx 3.18$ in this case, could only be established for chain lengths exceeding $N = 200$). Thus, in the present work we have thoroughly studied the temperature range $3.0 \le T \le 4.0$. From previous work[46] on rather long chains in polymer brushes on flat surfaces, using the same model (Eqs. (1) and (2)) to describe the interactions, it is known that for $T = 4.0$ one finds a behavior characteristic for (moderately) good solvents. Very good solvent conditions could be obtained from a slightly different model that has extensively been studied for standard polymer brushes,[36,47] where in Eq. (1) the cutoff is chosen to coincide with the minimum of the potential, $r_c = 2^{1/6}\sigma_{LJ}$ (and then also $T = 1$ can be chosen for this essentially athermal model). Rather

than carrying out simulations for bottle-brushes using this model, we found it more appropriate to compare to the athermal version of the bond fluctuation model on the simple cubic lattice, which describes very good solvent conditions[48,49] and has been used in our earlier work.[6,10,26] The use of this model has several advantages: (i) due to the fact that excluded volume constraints can be monitored via the occupancy of lattice sites, a very efficient implementation of the pivot algorithm in this Monte Carlo approach has become possible.[50] Therefore, very large bottle-brush polymers can be equilibrated, up to $N_b = 1027$, a task that is very difficult to achieve by molecular dynamics (MD) methods. (ii) The extent to which the bond fluctuation model and MD results agree (for comparable choices of parameters) yields some insight to what extent the pre-asymptotic regime that we study is model dependent. Of course, a truly universal behavior (apart from amplitude prefactors) can only be expected for the asymptotic regime where the side chain length $N \to \infty$, that is not accessible in simulations or experiments. One could ask why we do not use versions of the bond fluctuation model where an effective attraction between monomers is included[51] to study the effect of variable solvent quality in the framework of this model. The reason is that for temperatures slightly below the theta temperature already practically frozen configurations of monomers occur, with several monomers next to each other blocking any possibility to move. Thus the convergence towards equilibrium then is extremely slow.

However, since the application of the athermal version of the bond fluctuation model (BFM) to the simulation of bottle-brush polymers is well documented (Hsu and Paul[50] have given a careful discussion on the effort needed for the BFM to sample equilibrium properties) in the recent literature,[10,26,50] we do not give any details here.

In the MD simulation, the positions $\vec{r}_i(t)$ of the effective monomers with label i evolve in time t according to Newton's equation of motion, amended by the Langevin thermostat[33–36,39,40]

$$m_{LJ}\frac{d^2\vec{r}_i(t)}{dt^2} = -\nabla U_i(\{\vec{r}_j(t)\}) - \gamma\frac{d\vec{r}_i}{dt} + \vec{\Gamma}_i(t), \qquad (3)$$

where $U_i(\{\vec{r}_j(t)\})$ is the total potential acting on the ith bead due to its interactions with the other beads at sites $\{\vec{r}_j(t)\}$, γ is the friction coefficient, and $\vec{\Gamma}_i(t)$ is the associated random force. The latter is related to γ by the fluctuation-dissipation relation

$$\langle \vec{\Gamma}_i(t) \cdot \vec{\Gamma}_j(t) \rangle = 6k_B T \frac{\gamma}{m_{LJ}} \delta_{ij}\delta(t - t'). \qquad (4)$$

Following previous work[31–36] we choose $\gamma = 0.5$, the MD time unit

$$\tau_{LJ} = \left(\frac{m_{LJ}\sigma_{LJ}^2}{\varepsilon_{LJ}}\right)^{1/2}, \qquad (5)$$

being also unity, for our choice of units. Equation (3) was integrated using the leap frog algorithm,[52] with a time step $\delta t = 0.006\ \tau_{LJ}$, and utilizing the GROMACS package.[53] For the calculation of properties of the bottle-brushes, typically 500 statistically independent configurations are averaged over.

Of course, for bottle-brushes with large N_b equilibration of the polymer conformations is a difficult problem. Since we expect that end-to-end distance R_e and gyration radius R_g of the whole molecule belong to the slowest relaxing quantities, we studied the autocorrelation function of R_g^2 to test for equilibration,

$$\phi(t) = \frac{\left\langle \left(R_g^2(t'+t) - \overline{R_g^2}\right)\left(R_g^2(t') - \overline{R_g^2}\right)\right\rangle}{\left\langle \left(R_g^2(t') - \overline{R_g^2}\right)^2\right\rangle}. \qquad (6)$$

Note that $\overline{R_g^2}$ means an average of $R_g^2(t')$ over the time t' in the MD trajectory (and the average $\langle \cdots \rangle$ is computed by averaging over 500 statistically independent runs). Despite a substantial investment of computer time, $\phi(t)$ still exhibits significant fluctuations (remember that quantities such as R_e and R_g are known to exhibit a "lack of self-averaging,"[54,55] irrespective of how large N_b is). Figure 1 gives some examples for $\phi(t)$. If the number of samples would be infinite and $\delta t \to 0$, we should expect a monotonous decay of $\phi(t)$ towards zero as t becomes large. Due to the fact that the number of samples is not extremely large, and δt is not extremely small, Fig. 1 gives clear evidence for noise that is still correlated. We see that for small N the noise amplitude starts out at ± 0.1, and the time scale on which the fluctuations of $\phi(t)$ change sign is at $t \approx 1500\tau_{LJ}$ in (a), $t \approx 10000\tau_{LJ}$ in (b), and $t \approx 20000\tau_{LJ}$ in (c). While in cases (a) and (b), the (statistically meaningful) initial decay of $\phi(t)$ occurs so fast that it can only be seen on a magnified abscissa scale (inserts), we see that in (c) the initial decay is also much slower, and the associated time scale is of the same order as the time over which fluctuations are correlated. We have carefully considered $\phi(t)$ for all cases studied, and we have concluded that for our largest system studied (shown in Fig. 1(c), with a total number of 8000 effective monomers) the statistical effort is not yet sufficient to allow meaningful conclusions on the overall linear dimensions of the bottle-brush, while in all other cases the effort was judged to be sufficient. The damped oscillatory character of the relaxation seen particularly in Fig. 1(c) could be a matter of concern; we attribute this relaxation behavior to particular slow collective motions (breathing-type modes) of the chain.

Figure 2 shows a small selection of snapshot pictures of equilibrated bottle-brush polymers. From these snapshot pictures, it is already clear that the side chains cause a significant stiffening of the backbone, at least on a coarse-grained scale, and that bottle-brushes where N_b is not very much larger than N look like wormlike chains. This conclusion corroborates pictures generated experimentally (by atomic force microscopy or electron microscopy techniques, e.g., Refs. 1, 4, and 56), but this observation should not mislead one to claim that the Kratky-Porod wormlike chain model[57] often employed to analyze such micrographs provides an accurate description of bottle-brush polymers as we shall see.

Of course, both the bead-spring model and the BFM are idealizations of realistic comb-branched polymers, where also bond-angle potentials and torsional potentials are present and contribute to the local chain stiffness. Thus it is gratifying to note that nevertheless measured structure factors of real
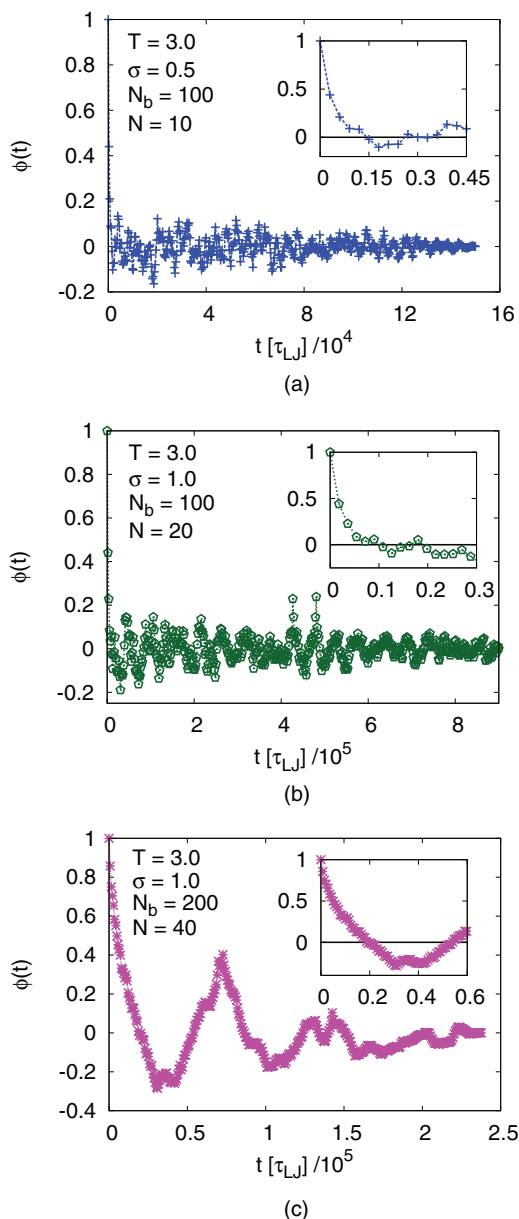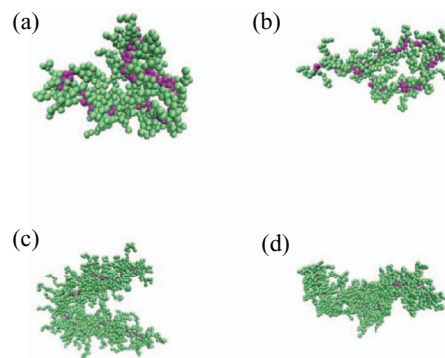
FIG. 2. Selected snapshot pictures of equilibrated configurations of bottle-brush polymers. Backbone monomers (when visible) are displayed in magenta (darker grey) color, side chain monomers in green (lighter grey). Cases shown refer to $\sigma = 0.5$, $N_b = 100$, $N = 10$, $T = 3.0$ (a) and $T = 4.0$ (b), as well as $\sigma = 1.0$, $N_b = 100$, $N = 20$, $T = 3.0$ (c) and $T = 4.0$ (d).
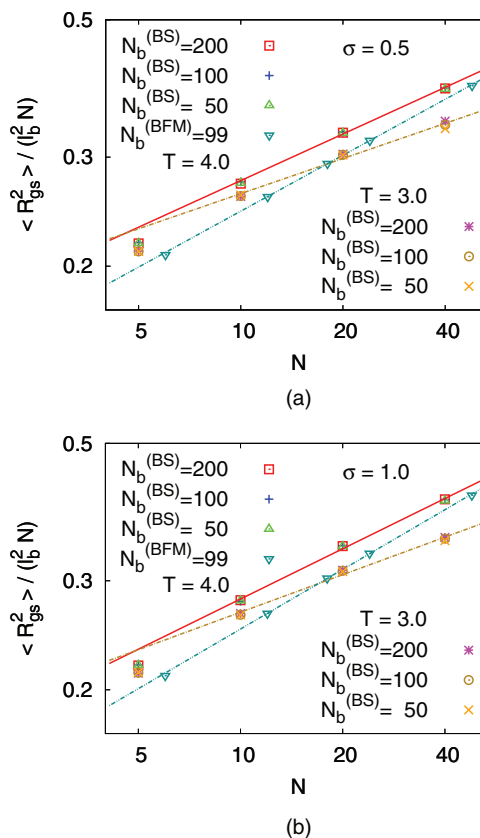

FIG. 1. Plot of $\phi(t)$ (see Eq. (6)) versus the time t in units of τ_{LJ}. Several cases are shown: $\sigma = 0.5$, $N_b = 100$, $N = 10$, $T = 3.0$ (a); $\sigma = 1.0$, $N_b = 100$, $N = 20$, $T = 3.0$ (b); and $\sigma = 1.0$, $N_b = 200$, $N = 40$, $T = 3.0$ (c). The fluctuations of $\phi(t)$ change sign initially at $t \approx 1500\tau_{LJ}$ (a), $t \approx 10000\tau_{LJ}$, and $t \approx 20000\tau_{LJ}$ (c) as shown in the inserts.

bottle-brush polymers[42] can be mapped almost quantitatively to their simulated BFM counterparts,[26] if the lattice spacing is fixed at a length of a few angstroms, and about three chemical monomers are mapped onto two effective monomers of the BFM. Residual minor discrepancies may, to some extent, be due to solvent quality effects.[26]

III. SIDE-CHAIN AND BACKBONE LINEAR DIMENSIONS AND ATTEMPTS TO EXTRACT "THE" PERSISTENCE LENGTH OF BOTTLE-BRUSH POLYMERS

Figure 3 presents log-log plots of the normalized mean square gyration radius of the side chains $\langle R_{gs}^2 \rangle / (l_b^2 N)$ as a

FIG. 3. Log-log plot of mean square radius of gyration of the side chains normalized by their chain length and by the square bond length l_b^2 between successive monomers, $\langle R_{gs}^2 \rangle / (l_b^2 N)$, versus side chain length N, for $\sigma = 0.5$ (a) and $\sigma = 1.0$ (b). Data for the bead-spring model at two temperatures ($T = 3.0$ and $T = 4.0$), as indicated in the figure are included, as well as three backbone chain lengths ($N_b = 50$, 100, and 200, respectively). For comparison, also data for the athermal bond fluctuation model for comparable backbone chain length are included. Straight lines indicate effective exponents $\nu_{\rm eff} \approx 0.60$ ($T = 3.0$) or $\nu_{\rm eff} \approx 0.63$ ($T = 4.0$) in case (a), and $\nu_{\rm eff} \approx 0.60$ ($T = 3.0$) or $\nu_{\rm eff} \approx 0.64$ ($T = 4.0$) in case (b). For the bond fluctuation model under very good solvent conditions the slightly larger effective exponent ($\nu_{\rm eff} \approx 0.65$ for $\sigma = 0.5$, and $\nu_{\rm eff} \approx 0.66$ for $\sigma = 1.0$) than for the off-lattice model with $T = 4.0$ results.
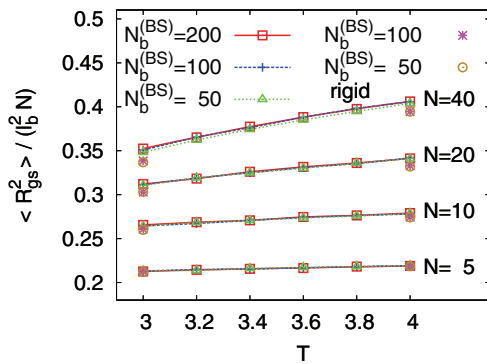
FIG. 4. Temperature dependence of the normalized mean square radius of gyration $\langle R_{gs}^2\rangle/(l_b^2 N)$ for four chain lengths ($N = 5, 10, 20,$ and 40), and three backbone lengths ($N_b = 50, 100,$ and 200), respectively. All data are for the bead-spring model and $\sigma = 1$. Data for bottle-brush polymers with flexible backbone are connected by curves to guide the reader's eyes. Data are only shown for $T = 3.0$ and 4.0 for the rigid backbone case.

function of side chain length N (l_b is the bond length between successive monomers), comparing data for grafting densities $\sigma = 0.5$ and $\sigma = 1.0$, and two temperatures ($T = 3.0$ and $T = 4.0$, respectively). Three different backbone lengths ($N_b = 50, 100,$ and 200) are included, but the dependence of the data on backbone length is not visible on the scale of the graph. Such a dependence on N_b would be expected due to effects near the chain ends of the backbone: in Ref. 26, it was shown that there is less stretching of the side chains in the direction perpendicular to the backbone near the chain ends of the backbone than in the central part of the backbone. However, this effect is almost completely compensated by the fact that side chains near the backbone chain ends are more strongly stretched in the direction of the backbone (side chains then are oriented away from the backbone chain ends). This fact has already been seen for bottle-brushes with rigid backbone but free ends.[58]

We have also checked that for the bead-spring model average side chain linear dimensions for bottle-brushes with rigid and flexible backbones are identical for the bond fluctuation model, at least in the accessible parameter regime. For the bond fluctuation model a similar equivalence has been found also for the radial density profile of the monomers.[59] Figure 4 shows then the temperature dependence of $\langle R_{gs}^2\rangle$ for the different choices of N, demonstrating that the side chain extension is independent of N_b and agrees well between rigid and flexible backbones. The small deviations observable between the rigid and the flexible backbone cases for large N are due to residual systematic errors of the simulations for the flexible backbone. The present work, therefore, suggests that the equivalence between bottle-brushes with rigid and flexible backbones carries over to chains in variable solvent quality, down to the theta point (but we caution the reader that this equivalence will break down for poor solvents, in the regime of intermediate grafting densities where for rigid backbones pearl-necklace structures occur[31,32]).

The straight lines on the log-log plots in Fig. 3 illustrate the empirical power law

$$\langle R_{gs}^2\rangle \propto N^{2\nu_{\text{eff}}},\qquad(7)$$

consistent with corresponding experiments (see Refs. 1 and 4 and references quoted therein) and we find that ν_{eff} decreases with decreasing solvent quality and with decreasing grafting density. In the good solvent regime, $\nu_{\text{eff}} > \nu = 0.588$,[60] the established value of the exponent describing the swelling of linear polymers under good solvent conditions, $R_g(N) \propto N^\nu$ for $N \to \infty$.[8,9] As expected, ν_{eff} is still distinctly smaller than the value predicted from scaling,[3] $\nu_{\text{eff}} = 2\nu/(1 + \nu) \approx 0.74$ or SCFT,[19] $3/4$. But the slight enhancement of ν_{eff} with respect to its value for free chains ($\nu = 1/2$ at the theta point, $T = 3.0$; $\nu = 0.588$ for good solvents) is evidence that the side chains interact with each other, which is a prerequisite for the expected induced stiffening of the backbone chain.

We now turn to the backbone linear dimensions. Here, we first caution the reader that in good solvent conditions we clearly also expect that the mean square end-to-end distance of a bottle-brush polymer satisfies the standard scaling relation

$$\langle R_{eb}^2\rangle \propto N_b^{2\nu},\quad \nu = 0.588,\quad N_b \to \infty,\qquad(8)$$

but the longer the side chain length the larger N_b must be chosen such that Eq. (8) can be verified. We start the discussion with data from the bond fluctuation model, where (for $N \le 24$) data up to $N_b = 1027$ are available.[10] Figure 5 hence shows a log-log plot of $\langle R_{eb}^2\rangle/(2l_b^2 N_b^{2\nu})$ versus N. The factor of 2 in the denominator is arbitrarily chosen, since for Gaussian chains ($\nu = 1/2$) the result would simply be the persistence length l_p in units of the bond length.[10] Thus, it was suggested[10] that
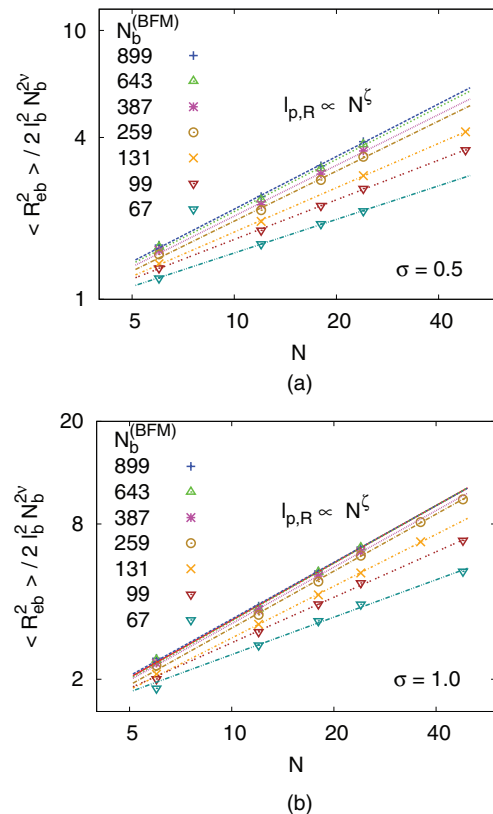

FIG. 5. Log-log plot of $\langle R_{eb}^2\rangle/(2l_b^2 N_b^{2\nu}) = \ell_{p,R}/\ell_b$ versus side chain length N, for the bond fluctuation model with $\sigma = 0.5$ (a) and $\sigma = 1.0$ (b) including different choices of N_b as indicated.
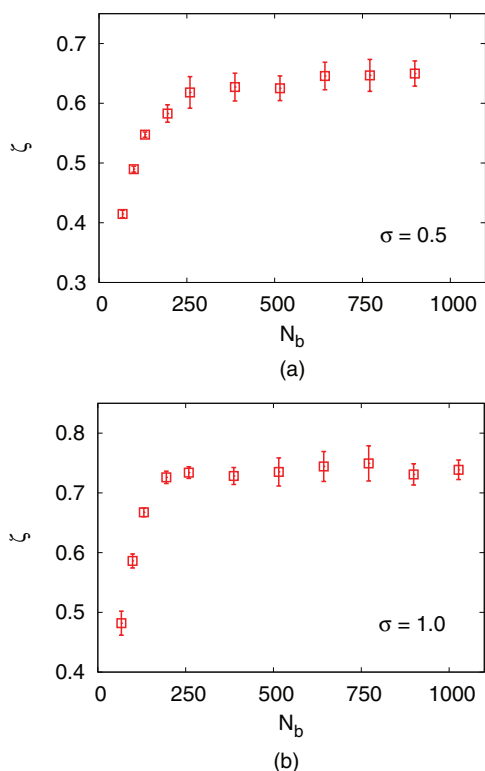
FIG. 6. Plot of the effective exponent ζ, extracted from the slope of the straight lines in Fig. 5, versus the backbone chain length N_b for $\sigma = 0.5$ (a) and $\sigma = 1.0$. All data are for the athermal bond fluctuation model.

in the excluded volume case one could introduce an effective persistence length $l_{p,R}(N)$ via the definition

$$l_{p,R}(N) = \langle R_{eb}^2 \rangle / \left(2 l_b N_b^{2\nu} \right), \quad N_b \to \infty . \tag{9}$$

Then Fig. 5 can be interpreted as a plot of $l_{p,R}(N)/l_b$ versus N in the region where it is basically independent of N_b. The quantity $l_{p,R}(N)$ defined in this way is compatible with an effective power law,

$$l_{p,R}(N) \propto N^\zeta , \tag{10}$$

but the effective exponent ζ clearly depends on N_b, if N_b is not chosen large enough (Fig. 6). Thus, Fig. 5 clearly shows that $l_{p,R}(N)$ is not a quantity characterizing the intrinsic stiffness of a bottle-brush polymer. For large N_b, the exponent ζ seems to saturate at a value close to 0.65 and 0.74 for $\sigma = 0.5$ and $\sigma = 1.0$, respectively, but for chain lengths N_b in the range from $N_b = 67$ to $N_b = 131$ it is only in the range from $\zeta = 0.41$ to $\zeta = 0.55$ and from $\zeta = 0.48$ to $\zeta = 0.67$ for $\sigma = 0.5$ and $\sigma = 1.0$, respectively.

Thus, it is no surprise that for the bead-spring model choosing $N_b = 50$, 100, or 200 values of this effective exponent ζ in a similar range are found (Fig. 7). Of course, one must be aware that there is no strict one-to-one correspondence[61] between the meaning of chain lengths N_b and N in different models: actually there may be the need for conversion factors $N_b^{(BFM)}/N_b^{(BS)}$ and $N^{(BFM)}/N^{(BS)}$ between the BS model and the BFM. The same fact is true when we compare simulations to experiments; e.g., the data of Rathgeber *et al.*[42] could be mapped to the BFM (Ref. 26) implying an equivalence between $N_b^{(exp)} = 400$ and $N_b^{(BFM)} = 259$ and
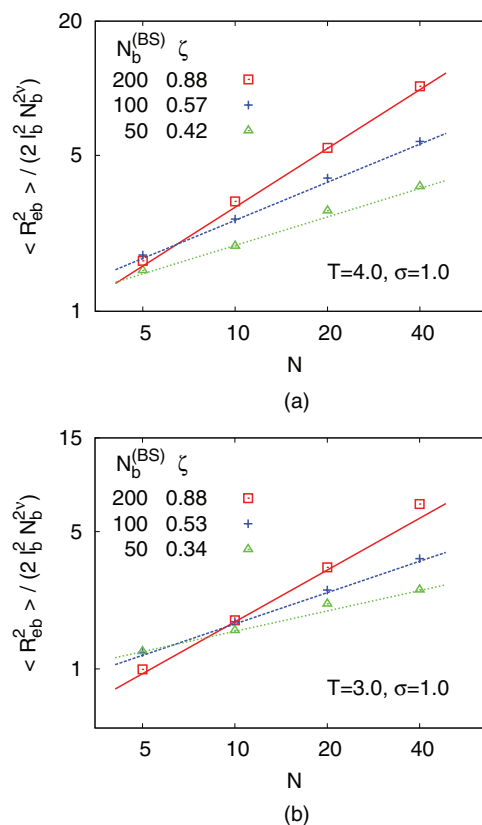

FIG. 7. Log-log plot of $\langle R_{eb}^2 \rangle / (2 l_b^2 N_b^{2\nu}) = \ell_{p,R}/\ell_b$ versus N. All data are for the bead-spring model with $\sigma = 1.0$ at both $T = 4.0$ (a) and $T = 3.0$ (b). Three backbone lengths are shown as indicated.

between $N^{(exp)} = 62$ and $N^{(BFM)} = 48$, for instance. We also note that with decreasing temperature $\langle R_{eb}^2 \rangle$ decreases, irrespective of N (and also ζ decreases). Again we remind the reader that this parameterization of our data in terms of effective exponents (also used in related experimental work[17,42]) only can serve to indicate the place in an extended crossover region to which the data belong.

When we analyze the gyration radius of the backbone as a function of backbone chain length for the BS model (Fig. 8) we find that over a restricted range of N_b one can fit the data by effective exponents again, $\langle R_{gb}^2 \rangle^{1/2} \propto N_b^{\nu_{eff}}$, with $0.55 \leq \nu_{eff} \leq 0.95$, and it is seen that ν_{eff} increases systematically with side chain length N, and ν_{eff} for $T = 4.0$ is larger than for $T = 3.0$, for the same choice of N. Of course, this variation of the effective exponent is just a reflection of a gradual crossover from the rodlike regime ($\langle R_g^2 \rangle^{1/2} \propto N_b$) to the self-avoiding walk (SAW)-like behavior of swollen coils ($\langle R_g^2 \rangle^{1/2} \propto N_b^\nu$, with $\nu \approx 0.588$) in the good solvent regime ($T = 4.0$) or Gaussian-like coils ($\langle R_g^2 \rangle^{1/2} \propto N_b^{1/2}$) for the theta point ($T = 3.0$), respectively. Similar plots as in Fig. 8 but for the BFM are shown in Figs. 9(a) and 9(b). Due to the availability of equilibrated data for much longer backbone chain lengths N_b for the BFM, the plot of $\langle R_{gb}^2 \rangle / (2 l_b^2 N_b^{2\nu})$ versus N_b (Fig. 9(c)) indeed shows that the data settle down to a horizontal plateau implying that the asymptotic region, where Eq. (9) can be applied indeed is reached. Instead of R_{eb}^2 in Eq. (9), we use R_{gb}^2 such that the estimate of the N-dependent effective persistence
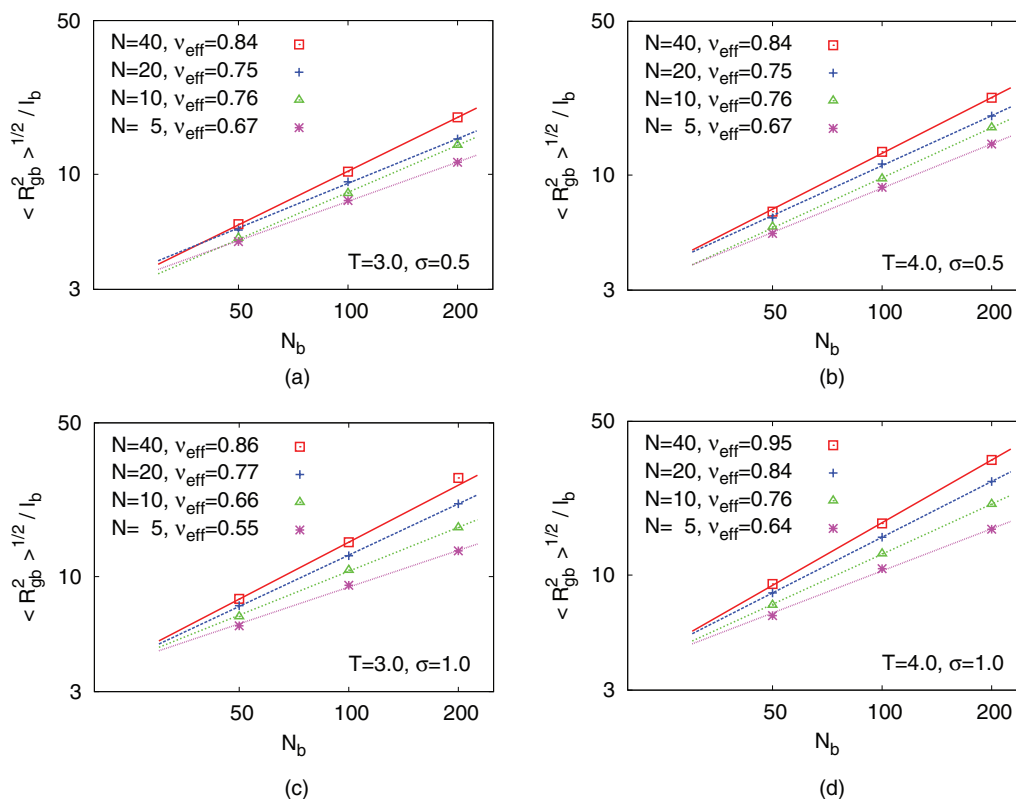
FIG. 8. Log-log plot of $\langle R_{gb}^2 \rangle^{1/2}/\ell_b$ versus backbone chain length N_b, for $\sigma = 0.5$ (a) (b) and $\sigma = 1.0$ (c) (d), including both $T = 3.0$ (a) (c) and $T = 4.0$ (b) (d), for the bead-spring model. Several side chain lengths N are included as indicated. Straight lines indicate a fit with effective exponents ν_{eff}.

length l_{p,R_g} is given by the horizontal line in Fig. 9(c). Actually, for fixed side chain length N the different choices of N_b can be collapsed on a master curve, when N_b is rescaled by s_{blob},[6] which can be interpreted as an estimate for the number of segments per persistence length. In our previous work,[6,11] we have shown that bottle-brushes under very good solvent conditions can be described as self-avoiding walks of effective "blobs," having a diameter that is just twice the cross-sectional radius of the bottle-brush, and containing a number s_{blob} of backbone monomers. Note that hence s_{blob} is not a fit parameter, but has been determined independently. This data collapse on a master curve is demonstrated for the BFM for the case $\sigma = 1$, $N = 6$, 12, 18, and 24 (Fig. 9(d)).

Since "the" persistence length of polymers in the standard textbooks[7–9] is traditionally defined from the decay of bond orientational correlations along the chains, we next focus on this quantity. Defining the bond vectors $\vec{a}_i$ in terms of the monomer positions $\vec{r}_i$ as $\vec{a}_i = \vec{r}_{i+1} - \vec{r}_i$, $i = 1, \ldots, N_b -1$, this bond orientational correlation is defined as

$$\langle \cos \theta(s) \rangle = l_b^{-2} \frac{1}{N_b - 1 - s} \sum_{i=1}^{N_b-1-s} \langle \vec{a}_i \cdot \vec{a}_{i+s} \rangle. \quad (11)$$

Note that $\langle \vec{a}_i^2 \rangle = l_b^2$ and hence $\langle \cos \theta(0) \rangle = 1$, of course. Considering the limit $N_b \to \infty$, and assuming Gaussian chain statistics, one obtains an exponential decay, since then $\langle \cos \theta(s) \rangle = \langle \cos \theta(1) \rangle^s = \exp[s \ln \langle \cos \theta(1) \rangle]$, and thus

$$\langle \cos \theta(s) \rangle = \exp[-s\ell_b/l_p], \quad l_p^{-1} = -\ln\langle \cos \theta(1) \rangle/\ell_b. \quad (12)$$

However, it has been shown by scaling and renormalization group arguments[62] and verified by simulations[10,11] that in the good solvent case there actually occurs a power law decay

$$\langle \cos \theta(s) \rangle \propto s^{-\beta}, \quad \beta = 2(1 - \nu) \approx 0.824, \quad s \to \infty, \quad (13)$$

while for chains at the theta point[63] or in melts,[64] one has

$$\langle \cos \theta(s) \rangle \propto s^{-3/2}, \quad s \to \infty. \quad (14)$$

As far as bond orientational correlations are concerned, Gaussian chain statistics hence is misleading for polymers, under all circumstances. However, Shirvanyants et al.[63] suggested that for semiflexible polymers (at the theta point), one can use still Eq. (12) but only for $1 \leq s \leq s^*$, where $s^* \propto l_p/l_b$ controls the crossover from the simple exponential decay, Eq. (12), to the power law, Eq. (14). Indeed, for a simple SAW model on the simple cubic lattice, where chain stiffness was controlled by an energy cost ε_b when the chain makes a $90°$ kink on the lattice,[11] it was shown that this suggestion[63] works qualitatively, also in the good solvent case, with $l_p \propto \exp(\varepsilon_b/k_B T)$ for $\varepsilon_b/k_B T \gg 1$, although the crossover between Eqs. (12) and (13) is not sharp but rather spread out over a decade in the variable s.

Motivated by this finding,[11] Figs. 10 and 11 hence present a few examples where $\langle \cos \theta(s) \rangle$ is plotted vs. s on a semi-log plot, to test for a possible applicability of Eq. (12) for not too large s. However, we find that in fact Eq. (12) does NEVER hold for small s ($s = 1, 2, 3$), unlike the semiflexible SAW model of Ref. 11, rather there occurs a very fast decay of $\langle \cos \theta(s) \rangle$ following a strongly bent curve (only two
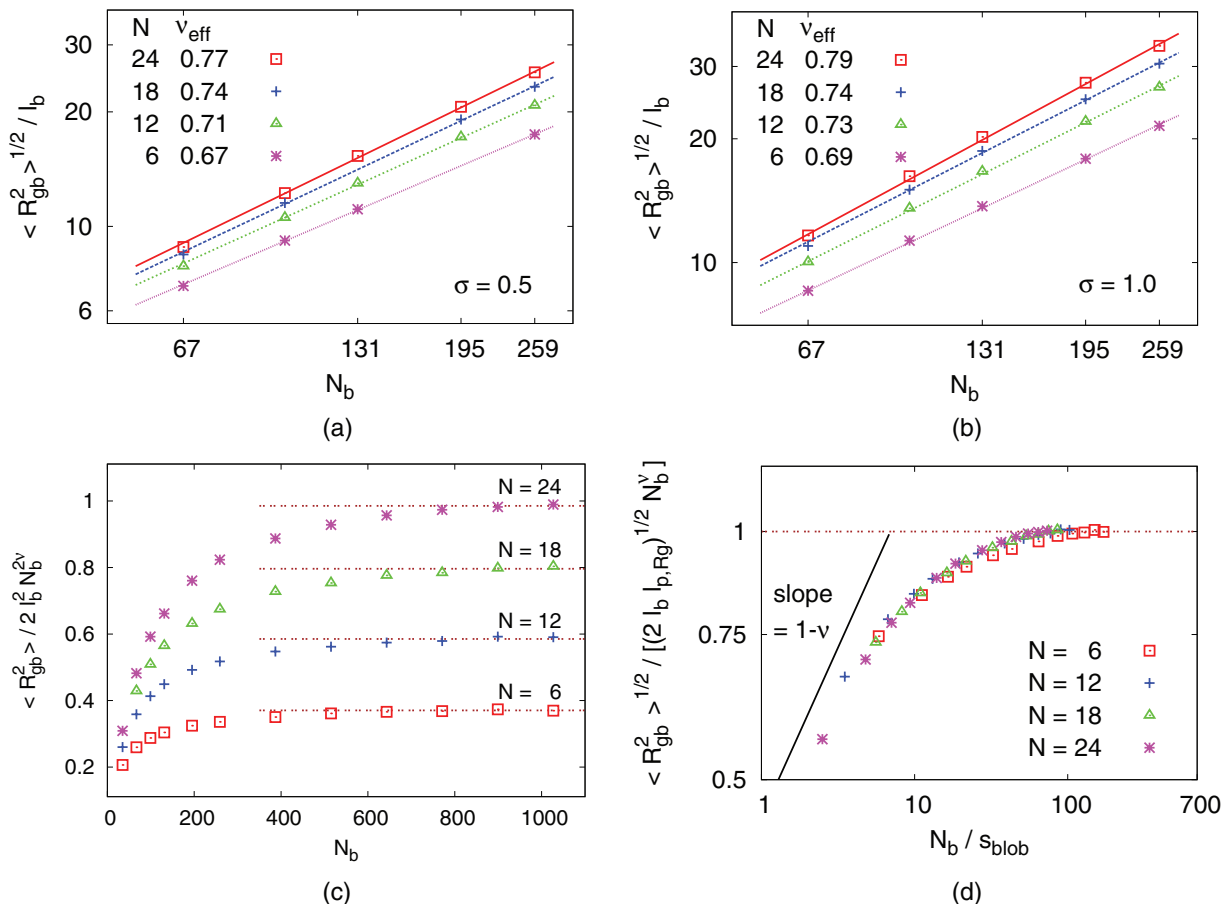
FIG. 9. Log-log plot of $\langle R_{gb}^2 \rangle^{1/2}/\ell_b$ for the bond fluctuation model versus backbone chain length N_b, for $67 \leq N_b \leq 259$, and several side chain lengths N, for $\sigma = 0.5$ (a) and $\sigma = 1.0$ (b). Part (c) shows the plot of rescaled radius of gyration $\langle R_{gb}^2 \rangle/(2l_b^2 N_b^{2\nu})$ of the bottle-brush polymers versus N_b for $\sigma = 1.0$. The persistence length $l_{p,Rg}$ is determined by the values of plateau. Part (d) shows a crossover scaling plot, collapsing for $N = 6$, 12, 18, and 24, $\sigma = 1.0$, and all data for $67 \leq N_b \leq 1027$ on a master curve, that describes the crossover from rods ($\langle R_{gb}^2 \rangle^{1/2} \propto N_b$) to swollen coils ($\langle R_{gb}^2 \rangle^{1/2} \propto N_b^\nu$, $\nu \approx 0.588$). For this purpose, N_b is rescaled with the blob diameter s_{blob}, which has been determined to be $s_{blob} = 6$, 10, 12, and 14 for $N = 6$, 12, 18, and 24, respectively.[6,11]

successive values of s can always be fit to a straight line, of course, but there is never an extended regime where a straight line through the origin, $\langle \cos \theta(s = 0) \rangle = 1$, would be compatible with the data). It is also remarkable that this initial behavior is almost independent of σ and N; an obvious interpretation is that the stiffening of the backbone caused by the presence of long side chains is effective only on mesoscopic length scales along the backbone, but not on the scale of a few subsequent backbone bonds, which maintain a high local flexibility. Only for $s \geq 4$, the data are compatible with a relation

$$\langle \cos \theta(s) \rangle = a \exp(-bs), \quad 4 \leq s \leq s_{max}, \quad (15)$$

where a and b are phenomenological constants, and s_{max} depends on both N, σ, and T distinctly (but cannot be accurately obtained from our simulations, because for $\langle \cos \theta(s) \rangle \leq 0.03$ the statistical accuracy of the data deteriorates.) Obviously, the relation (Eq. (12)) $l_p^{-1} = -\ln\langle \cos \theta(1) \rangle/\ell_b$ fails, but it seems tempting to identify an effective persistence length l_p^{eff} as $l_p^{\text{eff}}/\ell_b = b^{-1}$. However, when we would define the persistence length in this way, we obtain the result that l_p^{eff} depends on both N_b and on T, not only on the side chain length N and grafting density σ (Fig. 12 and Table I). For the bead-spring

model, one often estimates that the length unit ($\sigma_{\text{LJ}} = 1$) physically corresponds to about 0.5 nm. The data for $\ell_p^{\text{eff}}(T)$ at $\sigma = 1$ and good solvent conditions for $N_b = 200$ then would span a range from about 5 to about 40 nm, i.e., a similar range as proposed in recent experiments[17]. But already our previous work on the athermal bond fluctuation model[6,10,26] has given some evidence, that defining a persistence length from a fit of the data for $\langle \cos \theta(s) \rangle$ to Eq. (15) is not suitable to obtain a measure of the local intrinsic stiffness, since l_p^{eff} depends on N_b. The present data show that l_p^{eff} depends on T as well and, hence, is not just controlled by the chemical architecture of the bottle-brush (via the parameters, σ, N, and N_b), but depends on solvent conditions as well.

Thus, we argue that the physical significance of a persistence length l_p^{eff} extracted from bond orientational correlations in this way is very doubtful, even at the theta point. We also note that sometimes, due to curvature on the semi-log plot (e.g., Fig. 11(d)) such fits are ill-defined.

Finally, we consider the possible validity of the Kratky-Porod result for the end-to-end distance of the chains at the theta temperature, where for $N_b \rightarrow \infty$ we have (apart from logarithmic corrections) $\langle R_b^2 \rangle \propto N_b$, i.e., for this property a formula analogous to Gaussian chains holds. The Kratky-Porod result describes the crossover from rods to Gaussian
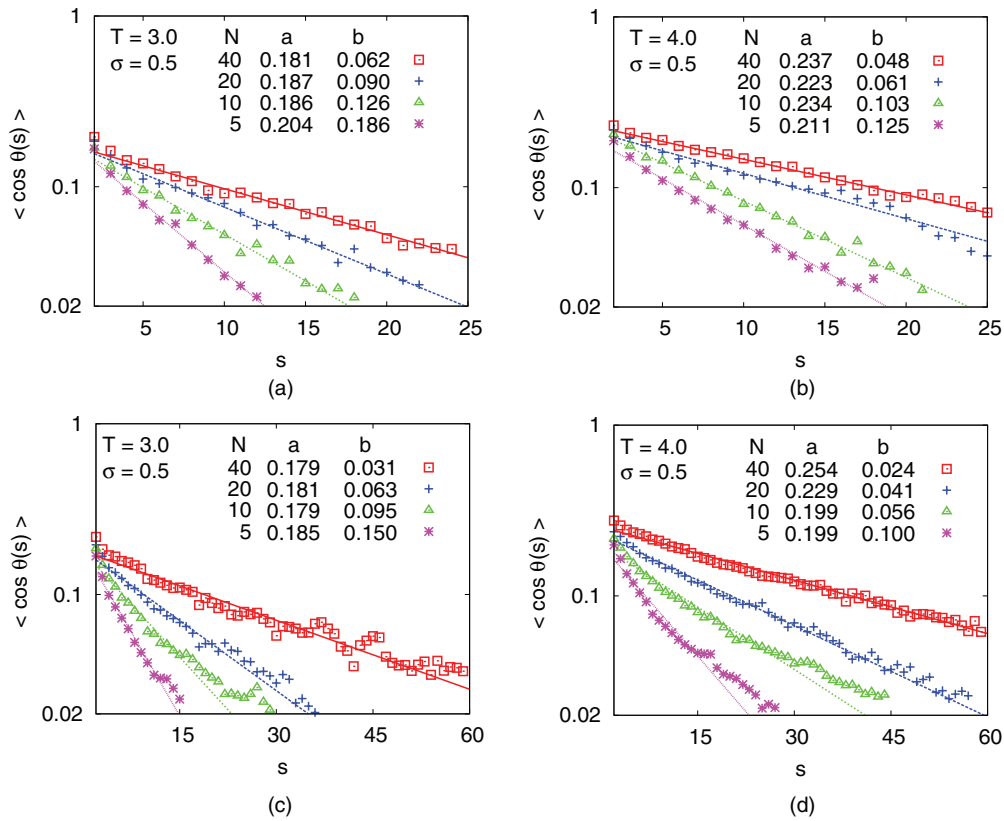
FIG. 10. Semi-log plot of $\langle \cos\theta(s) \rangle$ vs. s for the bead-spring model with $\sigma = 0.5$. Data are chosen for $N_b = 50$ (a) (b) and $N_b = 200$ (c) (d) at $T = 3.0$ (a) (c) and $T = 4.0$ (b) (d), respectively. Several choices of N are shown as indicated. Straight lines illustrate fits to a exp $(-bs)$, with constants a, b quoted in the figure.
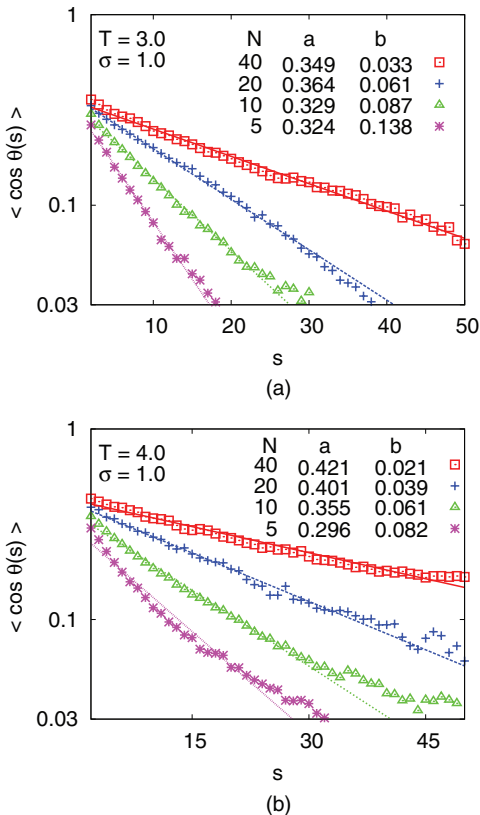

FIG. 11. Semi-log plot of $\langle \cos\theta(s) \rangle$ vs. s for the bead-spring model with $\sigma = 1.0$ and $N_b = 100$ at the temperatures $T = 3.0$ (a) and $T = 4.0$ (b), respectively. Several choices of N are shown as indicated. Straight lines illustrate fits to a exp $(-bs)$, with constants a, b as quoted in the figure.

chains,

$$\frac{\langle R_e^2 \rangle}{2 l_p L} = 1 - \frac{l_p}{L}[1 - \exp(-L/l_p)].\tag{16}$$

We can define an effective exponent $\nu_{\text{eff}}(L/l_p)$ in terms of the logarithmic derivative of this function, Figs. 13(a) and 13(b),

$$\frac{d \ln\left[\langle R_e^2 \rangle/(2 l_p L)\right]}{d \ln(L/l_p)} = 2\nu_{\text{eff}}(L/l_p) - 1.\tag{17}$$

Using the data for ν_{eff} at $N_b = 100$ from Figs. 8(a) and 8(c) (and similar data not shown for $\langle R_{eb}^2 \rangle$) we hence obtain estimates for the ratios L/l_p for the various choices of N for both $\sigma = 0.5$ and $\sigma = 1$. Note that the errors in our estimation of ν_{eff} translate into rather large errors in our estimates for L/l_p (both these errors of our data are indicated in Figs. 13(a) and 13(b)). Since we expect that the actual variation of $\langle R_{eb}^2 \rangle$ with N_b exhibits slight curvature (although this is hardly detected in Figs. 8(a) and 8(c)), we use only this intermediate value of $N_b = 100$ to estimate the relation between N and L/l_p, and we use neither $N_b = 50$ nor $N_b = 200$ for this purpose.

If the contour length L of the Kratky-Porod model, Eq. (16), would simply be the "chemical" contour length $L_{\text{ch}} = N_b l_b$, where the bond length l_b connecting two neighboring monomers along the backbone is $l_b \approx 1$, our results for L/l_p would readily yield explicit results for l_p. However, using then Eq. (16) to compute $\langle R_{eb}^2 \rangle/L^2$ yields an overestimation by about a factor of 5 for $\sigma = 1$. This discrepancy proves that L is significantly smaller than L_{ch}. Since Eq. (17) implies that there is a unique correspondence between ν_{eff} and the ratio ℓ_p/L, the factor of five discrepancy for $\langle R_e^2 \rangle$ (which is
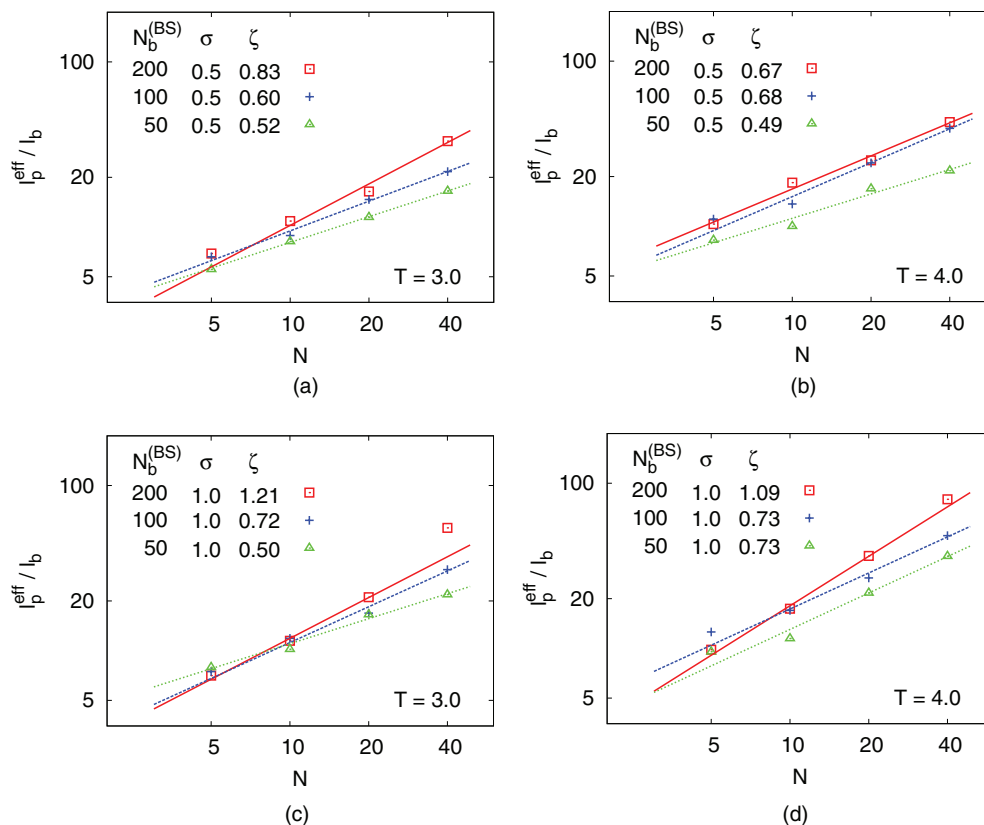
FIG. 12. Log-log plot of the effective persistence length $l_p^{\text{eff}}/\ell_b = b^{-1}$ as a function of side chain length N for $T = 3.0$ (a) (c) and $T = 4.0$ (b) (d) for several choices of N_b. Results for $\sigma = 1.0$ and $\sigma = 0.5$ are shown as indicated and the exponent estimates ζ extracted from the slope are listed. Values of l_p^{eff} are also listed in Table I.

TABLE I. Estimates of the effective persistence length $l_p^{\text{eff}} = b^{-1}\ell_b$ shown in Fig. 12 are listed for the BS model with the grafting densities $\sigma = 0.5$ and 1.0 at temperatures $T = 3.0$ and 4.0. Various values of the backbone length N_b and the side chain length N are chosen here. All length quoted in this table are given in units of ℓ_b (with $\ell_b \approx 0.97\sigma_{\text{LJ}}$). Note that ℓ_p^{eff} depends not only on N and σ, but also on N_b and T, and hence does not seem as a characteristic of intrinsic chain stiffness. Estimates of $l_p(N)$ shown in Fig. 13 are also listed for comparison.

		$\sigma = 0.5$		$\sigma = 1.0$	
N_b	N	l_p^{eff}/ℓ_b ($T = 3.0$)	l_p^{eff}/ℓ_b ($T = 4.0$)	l_p^{eff}/ℓ_b ($T = 3.0$)	l_p^{eff}/ℓ_b ($T = 4.0$)
50	5	5.38	8.00	7.69	9.26
50	10	7.94	9.71	9.90	11.14
50	20	11.12	16.39	16.05	21.01
50	40	16.03	21.27	21.19	35.09
100	5	6.41	10.73	7.25	12.20
100	10	8.26	13.33	11.52	16.47
100	20	14.25	23.47	16.37	25.91
100	40	21.01	38.46	38.03	47.62
200	5	6.71	10.00	6.85	9.52
200	10	10.55	17.83	11.14	16.95
200	20	15.92	24.33	20.45	35.21
200	40	32.15	41.49	53.76	77.52
	N	$l_p/\ell_b(T = 3.0)$		$l_p/\ell_b(T = 3.0)$	
	5	23.11		11.89	
	10	36.43		23.98	
	20	43.59		52.60	
	40	91.64		103.09	

proportional to the product of ℓ_p and L) means that both ℓ_p and L must be smaller by the same factor (at about $\sqrt{5}$). Thus we define $L = N_b l_b^{\text{eff}}$, where $l_b^{\text{eff}} (< 1)$ is interpreted as the average projection of a backbone bond on the direction of the coarse-grained contour of the wormlike chain. Thus we also can use the data shown in Figs. 13(a) and 13(b) to obtain explicit estimates for $l_p(N)$, taking into account $L = N_b l_b^{\text{eff}}$ instead of $L = N_b l_b$. Interestingly, the mechanisms leading to $l_b^{\text{eff}} < 1$ is also evident in the presence of the constant $a < 1$ in the fits of $\langle \cos \theta(s) \rangle = a \exp(- bs)$ in Figs. 10 and 11. Using then the estimates $l_b^{\text{eff}}(\sigma = 0.5) \approx 0.33$ and l_b^{eff} ($\sigma = 1) \approx 0.45$, the data for $\langle R_{eb}^2 \rangle / (2 l_p(N)L)$ at $T = 3.0$ are roughly compatible with Eq. (16), when we use $L/l_p(N)$ from Figs. 13(a) and 13(b) and take $L = l_b^{\text{eff}} N_b$ as is shown in Figs. 13(c) and 13(d). In this way, we have defined a correction factor $a_r = (l_b^{\text{eff}})^{-2}$ in Fig. 13, which was assumed to depend neither on N nor on N_b. Note that while only $N_b = 100$ was used in Figs. 13(a) and 13(b), data for $N_b = 50$, and 200 are included in Figs. 13(c) and 13(d). The resulting values of $l_p(N)$ which hence by construction do not depend on N_b (Table I) are considered to be the most reliable estimates for the considered model. However, we emphasize that Eq. (16) for bottle-brushes is useful only if the solution is at theta conditions, but not in the good solvent regime. Using the data for ν_{eff} at $N_b = 100$ from Figs. 8(a) to 8(c) (and similar data not shown for $\langle R_{eb}^2 \rangle$) we hence obtain estimates for the ratios L/l_p for the various choices of N for both $\sigma = 0.5$ and $\sigma = 1$.
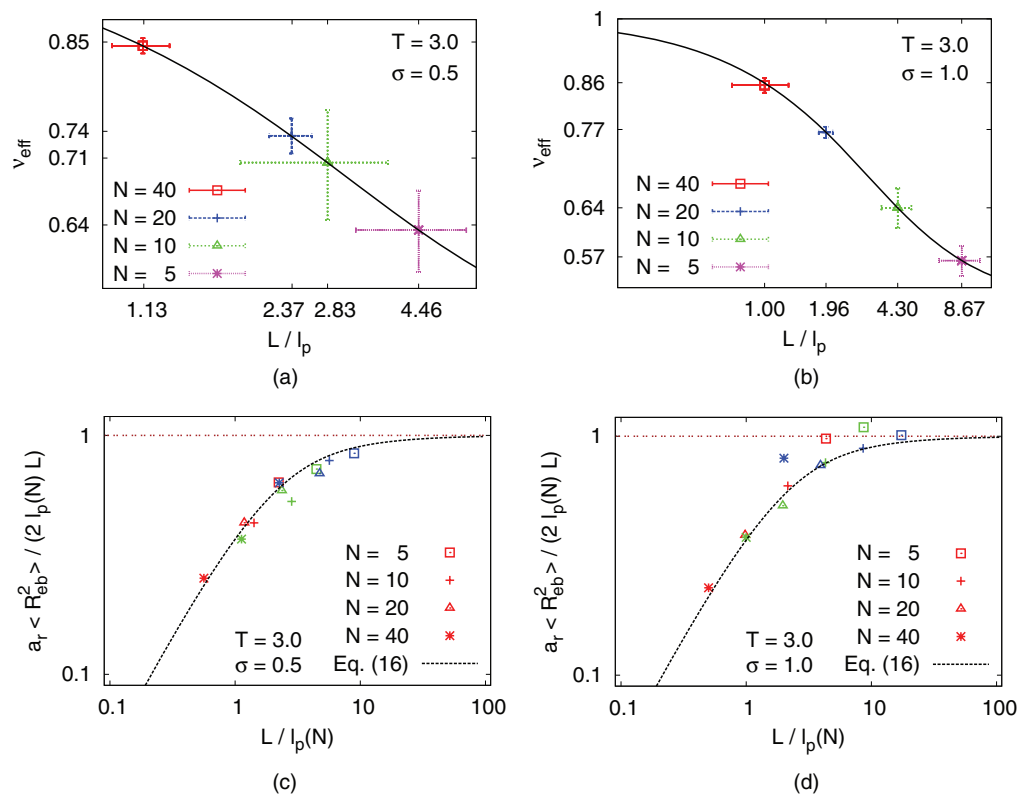
FIG. 13. Plot of the function $\nu_{eff}(L/l_p)$ versus L/l_p as predicted from the Kratky-Porod model, Eqs. (16) and (17) (full curves). The numbers for L/l_p extracted for $\sigma = 0.5$ (a) and $\sigma = 1.0$ (b) are quoted in the figure for various N at the abscissa. The average of the exponents ν_{eff} from Figs. 8(a) and 8(c) and from R_{eb}^2 (not shown) are quoted on the ordinate. Log-log plot of $a_r \langle R_{eb}^2 \rangle /(2l_p(N)L)$ vs. $L/l_p(N)$ for $\sigma = 0.5$ (c) and $\sigma = 1.0$ (d). Several choices of N are shown as indicated. Data plotted by the same symbol correspond to $N_b = 50$, 100, and 200 from left to right. The prediction for the Kratky-Porod model (Eq. (16)) is also shown for comparison. Approximate data collapse are obtained by introducing a factor of a_r ($a_r = 9.2 \pm 1.4$. and 4.9 ± 0.2 for $\sigma = 0.5$ and 1.0, respectively), cf. text. Values of $l_p(N)$ are also listed in Table I.

IV. CONCLUSIONS

In the present paper, a coarse-grained bead-spring model for bottle-brush polymers was studied by molecular dynamics methods, varying both the chain length N_b of the backbone and of the side chains (N), for two values of the grafting density, under variable solvent conditions. The main emphasis of the present work was a study of the various characteristic lengths describing the conformation of the macromolecule, contrasting the behavior under theta conditions with the behavior in the good solvent regime. Also a comparison with corresponding results for the bond fluctuation model has been performed; this athermal model represents very good solvent conditions, and while for corresponding parameters it yields results that are rather similar to the results for the bead-spring model in the good solvent regime, it has the advantage that much larger values of N_b can be studied.

Among the quantities that have been studied are the end-to-end distances of side chains and of the backbone, as well as the respective gyration radii, but also mesoscopic lengths that are particularly popular when a description in terms of the Kratky-Porod wormlike chain model is attempted, namely, "the" persistence length and "the" contour length of the wormlike chain. We have shown that for the range of rather short side chain lengths N that is only accessible, either in simulation or experiment, one often finds that a description in terms of power laws with effective exponents is adequate.

Specifically, the side chain radii vary as $\langle R_{gs}^2 \rangle^{1/2} \propto N^{\nu_{eff}}$, and $\nu_{eff} \approx 0.60$ (at the theta temperature $T = T_\theta$) or $\nu_{eff} \approx 0.63$ to 0.66 (in the good solvent regime), see Fig. 3. These effective exponents (for the present models with flexible backbones) are the same as for otherwise equivalent models with stiff backbones and also are practically independent of the backbone chain length. While the resulting effective exponents are systematically smaller than the asymptotic values predicted theoretically for the limit $N \to \infty$, $\nu \approx 0.74$ (good solvents) or $\nu = 2/3$ (theta solvents), respectively, they are comparable to the results of pertinent experiments: Zhang and co-workers[1,65] report $\nu_{eff} \approx 0.67$ for a bottle-brush, where the chemical nature of the main chain and the side chains is identical. For other systems exponents in the range $0.56 \leq \nu_{eff} \leq 0.67$ are reported,[17] again values comparable to our findings. Some experimental studies also report that somewhat different results occur when different solvents are used,[1,4,12,17,18] but a systematic variation of solvent quality to our knowledge has not yet been performed. Our results have shown that for $T \geq T_\theta$, the side chain radii vary only very weakly with temperature (which in our model causes the change in solvent quality), see Fig. 4.

Also the backbone end-to-end distance shows a power law variation with the side chain length, $\langle R_{eb}^2 \rangle \propto N^\xi$ (Figs. 5–7), reflecting thus the systematic backbone stiffening with increasing side chain length. In this case, however, the effective exponent depends on the backbone chain length N_b,

for $N_b \leq 300$, before a saturation at $\zeta \approx 0.65$ ($\sigma = 0.5$) or 0.75 ($\sigma = 1$) occurs, in the case of the bond fluctuation model. Even somewhat larger exponents are observed for the bead-spring model (up to $\zeta \approx 0.88$, Fig. 7).

A further effective exponent describes the variation of the backbone end-to-end distance and gyration radius with backbone chain length (Figs. 8 and 9). We have interpreted this variation as a crossover from rodlike behavior at small N_b to self-avoiding walk like behavior (under good solvent conditions) or random walk like behavior (under theta conditions) with increasing N_b.

Finally, "the" persistence length has been estimated in various ways, and demonstrating that the different estimates are not mutually consistent with each other, it was argued that a unique persistence length does not exist. While a regime of exponential decay of the bond autocorrelation function often can be observed over some intermediate range of contour distances (Figs. 10 and 11), the resulting estimates for a persistence length do not only depend on side chain length N and grafting density σ, but also on backbone chain length N_b and on temperature T (Fig. 12). However, when one studies the variation of the end-to-end distance of the backbone for $T = T_\theta$, an analysis in terms of the Kratky-Porod wormlike chain model (Eq. (16)) becomes feasible (Fig. 13). But one must not identify the contour length L implied by this model with the "chemical" contour length $L_{ch} = N_b l_b$, where l_b is the actual bond length, but rather one has $L = N_b l_b^{eff}$ with l_b^{eff} distinctly smaller than l_b. This effect results from the flexibility of the backbone on small scales; only on the scale of several backbone bonds does the stiffening due to the mutual side chain repulsions come into play. Thus, at the theta point both an effective contour length L and a persistence length $\ell_p(N)$ are well-defined quantities, in terms of a fit of the data to the Kratky-Porod model, while under good solvent conditions such an analysis is not appropriate.

We hope that the present work stimulates some more systematic experimental work on these issues. Of course, for real bottle-brushes where the chemical nature of the backbone often differs from the side chains, the interesting possibility arises that the backbone and the side chains have rather different theta temperatures. Another subtle issue concerns the precise location of theta conditions. While we expect that for the limit $N_b \to \infty$ at fixed ratio N/N_b, the theta conditions coincide with the theta conditions for simple linear polymers ($N_b \to \infty$, $N = 0$), it is not clear whether the location of the theta point for the limit $N_b \to \infty$ at fixed (small) N depends significantly on N. Thus, also more theoretical work clearly is needed.

[1]M. Zhang and A. H. E. Müller, J. Polym. Sci., Part A: Polym. Chem. **43**, 3461 (2005).
[2]A. V. Subbotin and A. N. Semenov, Polym. Sci., Ser. A **49**, 1328 (2007).
[3]H.-P. Hsu, W. Paul, and K. Binder, Macromol. Theory Simul. **16**, 660 (2007).
[4]S. S. Sheiko, B. S. Sumerlin, and K. Matyjaszewski, Prog. Polym. Sci. **33**, 759 (2008).
[5]I. I. Potemkin and V. V. Palyulin, Polym. Sci., Ser. A **51**, 123 (2009).
[6]H.-P. Hsu, W. Paul, and K. Binder, Macromol. Theory Simul. **20**, 510 (2011).
[7]P. J. Flory, *Statistical Mechanics of Chain Molecules* (Interscience, New York, 1969).
[8]A. Yu. Grosberg and A. R. Khokhlov, *Statistical Physics of Macromolecules* (American Institute of Physics, New York, 1994).
[9]M. Rubinstein and R. H. Colby, *Polymer Physics* (Oxford University Press, Oxford, 2003).
[10]H.-P. Hsu, W. Paul, and K. Binder, Macromolecules **43**, 3094 (2010).
[11]H.-P. Hsu, W. Paul, and K. Binder, Europhys. Lett. **92**, 28003 (2010).
[12]C. Li, N. Gunari, K. Fischer, A. Janshoff, and M. Schmidt, Angew. Chem. Int. Ed. **43**, 1101 (2004).
[13]*Proteoglycans: Structure, Biology, and Molecular Interactions*, edited by R. V. Iozzo (Marcel Dekker, New York, 2000).
[14]J. Klein, Science **323**, 47 (2009).
[15]K. Fischer, M. Gerle, and M. Schmidt, Proc. ACS, PMSE Anaheim **30**, 133 (1999).
[16]K. Fischer and M. Schmidt, Macromol. Rapid Commun. **22**, 787 (2001).
[17]B. Zhang, F. Gröhn, J. S. Pedersen, K. Fischer, and M. Schmidt, Macromolecules **39**, 8440 (2006).
[18]G. Cheng, Y. B. Melnichenko, G. D. Wignall, F. Hua, K. Hong, and J. W. Mays, Macromolecules **41** 9831 (2008).
[19]T. M. Birshtein, O. V. Borisov, E. B. Zhulina, A. R. Khokhlov, and T. A. Yurasova, Polym. Sci. U.S.S.R. **29**, 1293 (1987).
[20]Y. Rouault and O. V. Borisov, Macromolecules **29**, 2605 (1996).
[21]M. Saariaho, O. Ikkala, I. Szleifer, I. Erukhimovich, and G. ten Brinke, J. Chem. Phys. **107**, 3267 (1997).
[22]K. Shiokawa, K. Itoh, and N. Nemoto, J. Chem. Phys. **111**, 8165 (1999).
[23]P. G. Khalatur, D. G. Shirvanyanz, N. Yu. Starovoitova, and A. R. Khokhlov, Macromol. Theory Simul. **9**, 141 (2000).
[24]S. Elli, F. Ganazzoli, E. G. Timoshenko, Y. A. Kuznetsov, and R. Connolly, J. Chem. Phys. **120**, 6257 (2004).
[25]A. Yethiraj, J. Chem. Phys. **125**, 204901 (2006).
[26]H.-P. Hsu, W. Paul, S. Rathgeber, and K. Binder, Macromolecules **43**, 1592 (2010).
[27]L. Feuz, F. A. M. Leermakers, M. Textor, and O. V. Borisov, Macromolecules **38**, 8901 (2005).
[28]G. H. Fredrickson, Macromolecules **26**, 2825 (1993).
[29]S. S. Sheiko, O. V. Borisov, S. A. Prokhorova, and M. Möller, Eur. Phys. J. E **13**, 125 (2004).
[30]V. V. Vasilevskaya, A. A. Klochkov, P. G. Khalatur, A. R. Khokhlov, and G. ten Brinke, Macromol. Theory Simul. **10**, 389 (2001).
[31]P. E. Theodorakis, W. Paul, and K. Binder, Europhys. Lett. **88**, 63002 (2009).
[32]P. E. Theodorakis, W. Paul, and K. Binder, J. Chem. Phys. **133**, 104901 (2010).
[33]G. S. Grest and K. Kremer, Phys. Rev. A **33**, 3628 (1986).
[34]M. Murat and G. S. Grest, Macromolecules **22**, 4054 (1989).
[35]P. E. Theodorakis and N. G. Fytas, Soft Matter **7**, 1038 (2011).
[36]G. S. Grest and M. Murat, in *Monte Carlo and Molecular Dynamics Simulations in Polymer Science*, edited by K. Binder (Oxford University Press, New York 1995), p. 476.
[37]R. A. L. Vallée, W. Paul, and K. Binder, J. Chem. Phys. **132**, 034901 (2010); K. Binder, J. Baschnagel, and W. Paul, Prog. Polym. Sci. **28**, 115 (2003).
[38]G. S. Grest, Adv. Polym. Sci. **138**, 149 (1999); D. I. Dimitrov, A. Milchev, and K. Binder, J. Chem. Phys. **127**, 084905 (2007).
[39]*Simulation Methods for Polymers*, edited by M. Kotelyanskii and D. N. Theodorou (Monticello, New York, 2004).
[40]*Computational Soft Matter: From Synthetic Polymers to Proteins*, edited by N. Attig, K. Binder, H. Grubmüller, and K. Kremer (John von Neumann Institute for Computing (NIC), Jülich, Germany, 2004).

[41] S. Lecommandoux, F. Chécot, R. Borsali, M. Schappacher, A. Deffieux, A. Brûlet, and J. P. Cotton, Macromolecules **35**, 8878 (2002).

[42] S. Rathgeber, T. Pakula, A. Wilk, K. Matyjaszewski, and K. L. Beers, J. Chem. Phys. **122**, 124904 (2005).

[43] S. Bolisetty, C. Airaud, Y. Xu, A. H. E. Müller, L. Harnau, S. Rosenfeldt, P. Lindner, and M. Ballauff, Phys. Rev. E **75**, 040803(R) (2007).

[44] G. S. Grest and M. Murat, Macromolecules **26**, 3108 (1993).

[45] W. W. Graessley, R. C. Hayward, and G. S. Grest, Macromolecules **32**, 3510 (1999).

[46] T. Kreer, S. Metzger, M. Müller, K. Binder, and J. Baschnagel, J. Chem. Phys. **120**, 4012 (2004).

[47] K. Binder, T. Kreer, and A. Milchev, Soft Matter **7**, 7159 (2011).

[48] I. Carmesin and K. Kremer, Macromolecules **21**, 2819 (1988).

[49] H. P. Deutsch and K. Binder, J. Chem. Phys. **94**, 2294 (1991).

[50] H.-P. Hsu and W. Paul, Comput. Phys. Commun. **182**, 2115 (2011).

[51] N. B. Wilding, M. Müller, and K. Binder, J. Chem. Phys. **105**, 802 (1996).

[52] W. F. van Gunsteren and H. J. C. Berendsen, Mol. Simul. **1**, 173 (1988).

[53] Information about algorithms and implementation details for the Gromacs package can be found at http://www.gromacs.org; H. J. C. Berendsen, D. van der Spoel, and R. van Drunen, Comp. Phys. Comm. **91**, 43 (1995); E. Lindahl, B. Hess, and D. van der Spoel, J. Mol. Mod. **7**, 306 (2001).

[54] A. Milchev, K. Binder, and D. W. Heermann, Z. Phys. B **63**, 521 (1986).

[55] K. Binder and D. W. Heermann, *Monte Carlo Simulation in Statistical Physics: An Introduction*, 5th ed. (Springer, Berlin, 2010), Secs. 2.1.5 and 2.3.8.

[56] N. Gunari, M. Schmidt, and A. Janshoff, Macromolecules **39**, 2219 (2006).

[57] O. Kratky and G. Porod, J. Colloid Sci. **4**, 35 (1949).

[58] H.-P. Hsu, W. Paul, and K. Binder, J. Chem. Phys. **129**, 204904 (2008).

[59] H. P. Hsu, K. Binder, and W. Paul, Phys. Rev. Lett. **103**, 198301 (2009).

[60] J. C. Le Guillou and J. Zinn-Justin, Phys. Rev. B **21**, 3976 (1980).

[61] K. Binder, in *Monte Carlo and Molecular Dynamics Simulations in Polymer Science*, edited by K. Binder (Oxford University Press, New York, 1995), p. 1.

[62] L. Schäfer, A. Ostendorf, and J. Hager, J. Phys. A **32**, 7875 (1999).

[63] D. Shirvanyants, S. Panyukov, Q. Liao, and M. Rubinstein, Macromolecules **41**, 1475 (2008).

[64] P. Beckrich, A. Johner, A. N. Semenov, S. P. Obukhov, H. Benoit, and J. P. Wittmer, Macromolecules **40**, 3805 (2007).

[65] M. Zhang, T. Breiner, H. Mori, and A. H. E. Müller, Polymer **44**, 1449 (2003).